Title: New thiophene imines acting as hole transporting materials in photovoltaic devices

Author: Agnieszka Katarzyna Pająk, Paweł Gnida, Sonia Kotowicz, Jan Grzegorz Małecki, Marcin Libera, Katarzyna Bednarczyk, Ewa Schab-Balcerzak

Citation style: Pająk Agnieszka Katarzyna, Gnida Paweł, Kotowicz Sonia, Małecki Jan Grzegorz, Libera Marcin, Bednarczyk Katarzyna, Schab-Balcerzak Ewa. (2020). New thiophene imines acting as hole transporting materials in photovoltaic devices. "Energy & Fuels" 2020 (article ASAP), doi 10.1021/acs.energyfuels.0c01698

energy&fuels

pubs.acs.org/EF

Article

New Thiophene Imines Acting as Hole Transporting Materials in Photovoltaic Devices

Agnieszka Katarzyna Pająk, Paweł Gnida, Sonia Kotowicz, Jan Grzegorz Malecki, Marcin Libera, Katarzyna Bednarczyk, and Ewa Schab-Balcerzak*

Cite This: https://dx.doi.org/10.1021/acs.energyfuels.0c01698

Read Online

ACCESS | Metrics & More | Article Recommendations | Supporting Information

ABSTRACT: Five new unsymmetric thiophene imines end-capped with an electron-donating amine ($-NH_2$) group were obtained using a simple synthetic route, that is, the melt condensation of 2,5-diamino-thiophene-3,4-dicarboxylic acid diethyl ester with commercially available aldehydes. Their thermal stability and electrochemical and photophysical (absorption (UV−vis) and photoluminescence (PL)) properties were examined and density functional theory calculations were performed. The imines were thermally stable above 200 °C. They underwent reduction and oxidation processes and exhibited an energy band gap electrochemically estimated between 1.81 and 2.44 eV. They absorbed radiation from the UV and visible range to 480 nm and showed weak light emission. These compounds were investigated as hole transporting materials in solar cells with the structure FTO/b-TiO_2/m-TiO_2/perovskite/imine/Au. The highest photoelectric conversion efficiency was observed for compounds with a morpholine derivative substituent.

1. INTRODUCTION

In the past decades, increased interest in organic materials with unique properties and application possibilities in organic electronics, i.e., photovoltaics (OPVs), light emitting diodes (OLEDs), and field-effect transistors (FETs) has been observed. Despite appreciable development of optoelectronics in recent years, many problems related to semiconductor processing and the efficiency of the devices are still unresolved. Therefore, new stable, processable organic compounds that are able to meet the continually increasing demands are being sought.[1−13] Among the various π-conjugated compounds, azomethines have attracted broad research interest as components in optoelectronic devices.[7−15] Imines are synthesized under mild reaction conditions, where only water is formed as a byproduct (the reaction is not harmful to the environment), and do not require a complicated purification process and metal catalysts.[7−11,13] The possibility of modification of the azomethine structure through the appropriate selection of amines and carbonyl compounds allows for the preparation of new compounds with the desired properties. Considering the chemical structure of the investigated imines for organic electronics, special attention is paid to heterocyclic azomethines with a thiophene unit.[8−14] Compounds with a thiophene structure exhibit many desirable properties in optoelectronics, such as low oxidation potentials, low band-gap energy, good electrical conductivity, and chemical and thermal stability.[6,8−10,12,13] Apart from the various fields of imine applications, they are also investigated as materials for photovoltaic (PV) cells.[16−27] Nowadays, they are examined in bulk heterojunctions (BHJs),[16−29] dye-sensitized solar cells (DSSCs),[30] and perovskite solar cells (PSCs).[31−34] Bogdanowicz et al.[16] reported unsymmetrical and symmetrical azomethines with thiophene and thiazole structures tested in BHJ cells as donor components. Additionally, the effect of the azomethine weight ratio in the active layer on PV parameters was investigated. The highest power conversion efficiency (PCE) of about 0.42% for devices with the structure ITO/PEDOT:PSS/PTB7:symmetrical imine:$PC_{71}BM$(4:1):8/Al was indicated. Petrus et al.[17] applied two conjugated thiophene azomethines with the triphenylamine (TPA) moiety in BHJ PV devices (ITO/MoO_x/imine:PCBM (1:2)/LiF/Al) and registered a PCE of around 1.2%. Demeter et al.[18] examined push−pull imines with the thiophene core as the donor component with a fullerene acceptor in BHJ devices and the highest PCE was approximately 2%. Our research group also reported the results of applications of compounds with imine bonds in BHJ cells.[19−22,29] In the case of symmetrical molecules with two −N═CH− linkages end-capped with anthracene, phenanthrene, and pyrene, the highest PCE of about 0.21 and 0.30% was registered for the device based on imine and azine with pyrene units, respectively.[19] In turn, in a series of azomethines with one imine bond, the BHJ device with an active layer consists of azomethine with two anthracene units exhibiting the best value of PCE = 0.39%.[20] We also tested compounds containing both imine linkages and naphthalimide cores for application in devices with P3HT:PCBM.[21,22] The best photovoltaic parameters with PCEs of about 5.50 and 5.16% were obtained for cells bearing the active layer naphthalene

Received: May 27, 2020
Revised: July 21, 2020
Published: July 24, 2020

diimide-imines with the bithiophene and 3,4-ethylenedioxythiophene (EDOT) unit, respectively.[22] It should be noted that the achieved PCE was significantly higher compared to that of a reference cell based on a neat P3HT:PCBM. Unsymmetrical imines with benzothiazole units utilized as a donor unit in the device ITO/PEDOT:PSS/P3HT:PCBM:imine (1:1:1)/Al gave a low PCE of about 0.1%.[29] Among the various polyazomethines tested in BHJ devices,[23−28] the cells with polyimine bearing TPA units showed the highest PV performance. A PCE of about 0.49% for the device with the architecture ITO/PEDOT:PSS/polyimine:$PC_{71}BM$ (1:2)/Al was obtained.[28] An example of imine examination is when tris-4-iminophenyl-ethyl-thiophene is used as a sensitizer in a DSSC and the device shows an open circuit voltage and a short circuit current of about 0.62 V and 0.35 mA, respectively.[30] As mentioned earlier, imines were also applied as hole transporting materials (HTMs) in PSCs.[31−34] Petrus et al.[31,32] reported a series of imines with various cores (EDOT, thiophene, furan, TPA, and benzene) end-capped with the TPA unit employed in PSCs. The fabricated PSC exhibited a PCE in the broad range of 0.2−14.4% being the highest for imines consisting of EDOT end-capped with TPA. Gawlinska et al.[34] reported that HTMs applied two polyazomethines with thiophene rings. The best performance with a PCE of about 6.9% found for a device with fluorene moieties in the polyimine structure and was used in the following architectures of the device FTO/TiO_2/TiO_2/perovskite/S7/Au.

Inspired by the above findings, which show that imines can be perspective materials for organic photovoltaics, we synthesized a series of imines based on amine DAT (2,5-diamino-thiophene-3,4-dicarboxylic acid diethyl ester) to investigate the relationship between their chemical structures and properties crucial for optoelectronics applications. The synthesized imines were examined as HTMs in perovskite solar cells. In the given research, the effect of the chemical structure of unsymmetrical thiophene compounds with the imine bond on its thermal stability and electrochemical and photophysical behavior was determined. Additionally, frontier molecular orbitals, geometric structures, and electronic spectra were studied with the use of density functional theory (DFT) and time-dependent density functional theory (TD-DFT). The possibility of hydrogen bond formation in the as-prepared azomethines was investigated experimentally and theoretically using ^{1}H NMR and Fourier transform infrared (FTIR) spectroscopy and DFT, respectively.

2. EXPERIMENTAL SECTION

Materials used, ^{1}H NMR, ^{13}C NMR, and FTIR characterization, elemental analysis, and theoretical calculations are available in the Supporting Information.

2.1. Synthesis of Thiophene Imines. All imines were obtained using melt condensation. Aldehydes (0.5 mmol) (4-dimethylamino-benzaldehyde or 4-[(2-cyanoethyl)methylamino]benzaldehyde or 4-(4-morpholinyl)benzaldehyde or 3-quinolinecarboxaldehyde or 4-methylbenzaldehyde) were melted under an argon atmosphere, and 2,5-diamino-thiophene-3,4-dicarboxylic acid diethyl ester (0.25 mmol) was added. In the next step, after about 4 h, a few drops of DMA were added to the reaction mixture. After 24 h, the obtained product was dissolved in chloroform, then precipitated in hexane, and washed several times with hexane. Next, the imines were dried at 40 °C in a vacuum oven for 24 h.

2.2. Film Preparations. Films (0.02 g of imines in 1 cm^3 of solvent) were fabricated from a homogenous chloroform solution. The obtained mixtures were spin-coated on glass substrates. The films were dried for 24 h in a vacuum oven at 50 °C. Additionally, an FTO/b-TiO_2/m-TiO_2/perovskite/**Az-4** film similar to the devices was fabricated by the same method as that used in solar cell preparations and current−voltage (I−V) measurements.

2.3. Characterization Methods. Nuclear magnetic resonance (NMR) (^{1}H and ^{13}C NMR and HMQC) spectra of the obtained imines were measured on a Bruker AC400 spectrometer 400 MHz, with TMS as the internal standard and chloroform ($CDCl_3$) or dimethyl sulfoxide (DMSO-d_6) as solvents. FTIR was performed using a Thermo Scientific Nicolet iS5 in the range of 400−4000 cm^{-1}, where the KBr pressed pellets were dried before use for 10 min. Elemental analysis was performed using a Vario EL III apparatus (Elementar, Germany). The thermal stability was investigated on a PerkinElmer Pyris 1 TGA with a heating rate of 10 °C/min under a stream of nitrogen (20 mL/min) to 600 °C. Absorption spectra in the UV−vis range were recorded using a PerkinElmer Lambda Bio 40 UV/VIS spectrometer, and a Jasco V-550 spectrophotometer was used for recording the UV−vis spectra of films. PL spectra in both solutions ($CHCl_3$ and NMP) were recorded using a Varian Carry Eclipse Spectrometer. PL measurements for films were carried out using a Hitachi F-2500 spectrometer. Quantum yields (Φ_f) were measured on Edinburgh Instruments FLS 980 with the Avantes AvaSphere-80 integrating sphere. Edinburgh Instruments software allowed the absolute quantum yield measurements based on the direct measurement of the number of emitted and absorbed photons using the integrating sphere. For solutions, the pure solvent as a standard and the excitation wavelengths with the most intense luminescence were used. Redox properties were investigated on an Eco ChemieAutolab PGSTAT128n potentiostat with the Pt electrode (diam. 1.0 mm), the Pt coil, and the Ag wire as the working, auxiliary, and reference electrodes. As an internal standard, the ferrocene couple (Fc/Fc^+) was used. Experiments were performed in CH_2Cl_2 (ACROSS Organics, 99.9% for biochemistry grade) with 0.1 mol/dm^3 Bu_4NPF_6 (Aldrich, 99%) as the supporting electrolyte salt at temperature 23 ± 1 °C under argon purging. AFM micrographs were obtained using a Dimension ICON NanoScope IIId Bruker, operating in the tapping mode, in air.

2.4. Solar Cell Preparations and Current−Voltage (I−V) Measurements. The FTO glasses were cleaned with surfactant, deionized water, and isopropanol by ultrasonication. Afterward, a blocking layer b-TiO_2 (spin-coated tetraethyl orthotitanate in EtOH and HCl) was prepared on FTOs, as described in the paper.[35,36] The next step was a mesoporous m-TiO_2 layer being screen-printed on FTO/b-TiO_2 under certain conditions as discussed in the literature.[36] The two-step method was used to obtain the perovskite layer. In the first step, the hot solution of PbI_2 (in anhydrous *N*,*N*-dimethylformamide) was spin-coated on the FTO with TiO_2 layers. In the second step, the samples were dipped in a solution of MAI in isopropanol (using prewetting by IPA) and after this they were dried for an appropriate time.[36] The mixture of the thiophene core material solution was 72.3 mg of the thiophene compound in 1 mL of chlorobenzene, 28.8 μL of 4-*tert*-butyl pyridine, and 17.5 μL of lithium bis(trifluoromethanesulfonyl)imide (520 mg Li-TFSI in 1 mL acetonitrile). The foregoing solution was spin-coated on the FTO/b-TiO_2/m-TiO_2 at 4.000 rpm for 30 s.[36,37] On the as-prepared devices, the gold electrode was deposited by thermal evaporation (~10^{-6} mbar). Three devices were constructed for each tested compound as HTMs in perovskite solar cells.

The prepared devices were tested using a PET Photo Emission TechInc.Model SS 200AAA class solar simulator under standard test conditions (25 °C, 1000 W/m^2, AM1.5, active area was 0.25 cm^2).

3. RESULTS AND DISCUSSION

A series of new unsymmetric thiophene imines end-caped with an electron-donating amine (−NH_2) group were synthesized using the condensation of diamino-thiophene-3,4-dicarboxylic acid diethyl ester (DAT) with 4-dimethylamino-benzaldehyde, 4-[(2-cyanoethyl)methylamino]benzaldehyde, 4-(4-morpholinyl)benzaldehyde, 3-quinolinecarboxaldehyde, and

https://dx.doi.org/10.1021/acs.energyfuels.0c01698
Energy Fuels XXXX, XXX, XXX−XXX

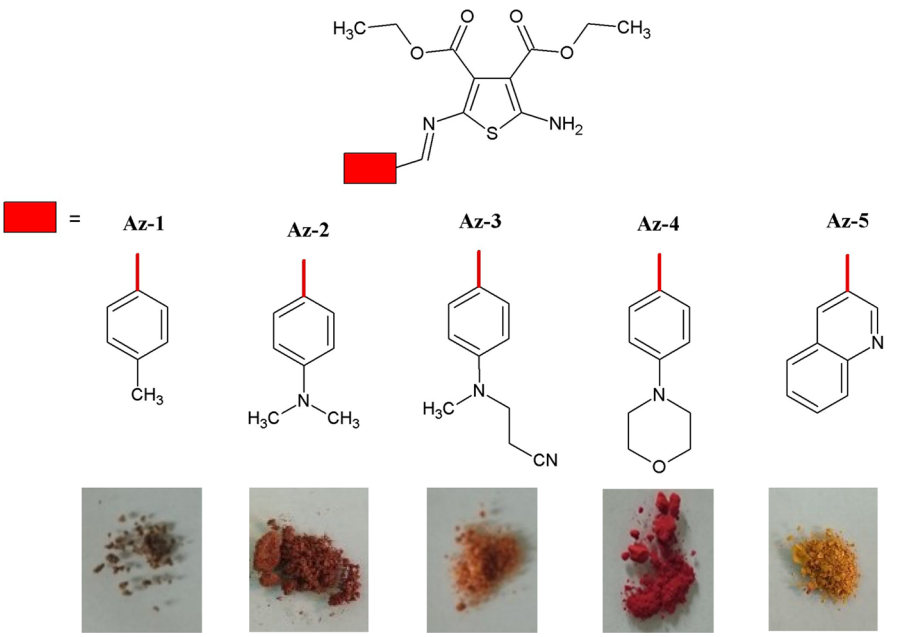

Figure 1. Chemical structures of thiophene imines and their photographs under daylight.

4-methylbenzaldehyde powders (cf. Figure 1). The influence of the chemical structure of the electron-donating substituent on the phenyl ring or the electron-accepting unit conjugated with the thiophene ring via azomethine linkages was considered.

3.1. Structural Analysis. Instrumental techniques including ^{1}H NMR, ^{13}C NMR, FTIR, and elemental analysis were performed to confirm the chemical structure and purity of the prepared imines. In the ^{1}H NMR spectra, the signal of the proton of the −HC═N− bond was observed in the range of 7.92 (**Az-2**)−8.32 (**Az-5**) ppm. The lack of the characteristic signal of the proton of the aldehyde group (−COH) confirmed the condensation reaction. The signal of amine protons ($-NH_2$) was observed from 7.73 ppm (**Az-2**) to 8.02 ppm (**Az-5**). The signals of the methyl ($-CH_3$) and methylene ($-CH_2-$) groups from DAT were recorded at about 1.20 and 1.30 ppm as a triplet and at 4.15−4.30 ppm as a quartet, respectively. Moreover, the signal for the methyl group (**Az-1**) was registered at 2.35 ppm and for **Az-2** of the $-N-CH_3$ group was registered at 3.00 ppm. However, for **Az-3**, the signal of the $-N-CH_3$ group was observed at 3.03 ppm and the signals of the two $-CH_2-$ groups (from $-N-CH_2-CH_2-CN$) were observed at 3.76 ppm and 2.75 ppm. The correlated ^{1}H-^{13}C HMQC spectra were obtained for **Az-5** and are presented in the Supporting Information Figure S1. The obtained HMQC spectra show the correlation of the proton signal from hydrogen at 8.31 ppm with the carbon atom (at 149.71 ppm) in the −HC═N− bond. In the FT-IR spectra of imines, an absorption band of the −HC═N− linkages from 1661 cm^{-1} (**Az-2**) to 1682 cm^{-1} (**Az-5**) was observed. The absorption of aromatic and aliphatic groups was observed in the range of 3029−3095 and 2828−2982 cm^{-1}, respectively. Furthermore, two absorption bands characteristic of $-NH_2$ were recorded at 3385−3443 and 3242−3330 cm^{-1}. The bands in the ester −C═O group in the range of 1702−1732 cm^{-1} were detected. The elemental analysis confirmed the purity of the synthesized azomethines.

The presence of the primary amine group and an oxygen atom in ester units in the synthesized azomethines creates the possibility of the hydrogen bond formation.[13,38] The presence of hydrogen bonds in exemplary imines (**Az-1**, **Az-3**, and **Az-5**) was theoretically studied using DFT. The calculated C−O···H−N distances, based on the optimized geometries, are almost the same in the given azomethines with a value close to 2.0 A° and an N−H···O angle of 125°, which are in line with the experimental values of 2.1 A° and 123° obtained for ethyl 2-amino-4-(4-methylphenyl)-5-(4-nitrophenyl)thiophene-3-carboxylate.[39] Almost the same geometrical parameters of the hydrogen bonds indicate similar energy of these interactions, as can be seen from the potential energy curves shown in Figure 2 and Supporting Information, Figure S2.The calculated H-bond stabilization energy is about 8.5 kcal/mol. Thus, the H-bonds can be formed in the investigated imines.

3.2. Thermal Stability. Thermogravimetric analysis (TGA) was performed to estimate the thermal stability of the synthesized azomethines. The thermal data are summar-

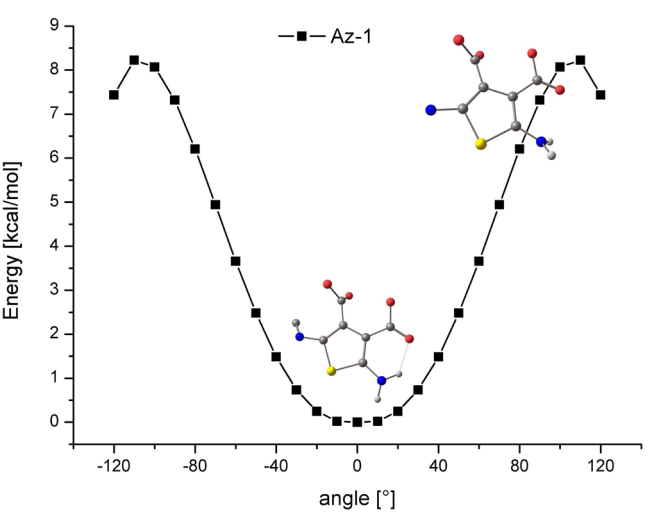

Figure 2. Potential energy profiles along the rotation of the amine group in the **Az-1**.

https://dx.doi.org/10.1021/acs.energyfuels.0c01698
Energy Fuels XXXX, XXX, XXX−XXX

ized in Table 1 and the corresponding TGA curves are given in Figure S3.

Table 1. TGA Data of the Obtained Imines

code	Az-1	Az-2	Az-3	Az-4	Az-5
T_5 [°C]	233	234	260	265	257
T_{10} [°C]	255	259	278	278	268
T_{max}[a] [°C]	262;376	375;355	282;363	282;363	270;372

[a]Temperature of the maximum decomposition rate from DTG thermograms.

The beginning of thermal decomposition estimated as temperature of 5 % weight loss (T_5) for methyl (**Az-1**) and dimethylamine (**Az-2**) group as substituent was lower about 30 °C in compare with **Az-3** - **Az-5**.[32]

3.3. Electrochemical Properties. The redox properties of **Az-1**−**Az-5** were investigated in dichloromethane (CH_2Cl_2) solution using a Pt coil as a working electrode and 0.1 M Bu_4NPF_6 as an electrolyte. To estimate the ionization potentials (IPs) and electron affinities (EAs), the differential pulse voltammetry (DPV) and cyclic voltammetry (CV) methods were used. The IP of the ferrocene couple (Fc/Fc^+) was equal to −5.1 eV based on the literature.[40] The reversibility of the electron transfer process was based on the difference between potential peaks (E_{pa} and E_{pc}, $\Delta E_p = E_{pa} - E_{pc}$). Considering EAs and IPs, the energy band gap (E_g) was estimated. Electrochemical results are provided in Table 2 and the CV voltammograms are shown in Figure 3.

The irreversible process of reduction was seen for imine with the methyl (**Az-1**) and (cyanoethyl)methylamino substituents (**Az-3**). The quasi-reversible process (ΔE_p < 100 mV) for compounds bearing the dimethylamino (**Az-2**), morpholine (**Az-4**), and quinoline (**Az-5**) structure was noted. The reversible process of oxidation based on the ΔE_p value (ΔE_p = 60 mV) was observed for **Az-3**. For **Az-2** and **Az-4**, the quasi-reversible oxidation process (ΔE_p < 90 mV) was observed. In the case of **Az-1** and **Az-5**, the oxidation process was irreversible. The oxidation onset potentials ($E_{ox}^{onsetCV}$) were in the range of 0.05−0.39 V, where the lowest potential was found for **Az-4** and a similar value ($E_{ox}^{onsetCV}$ = 0.09 V) for **Az-2** and **Az-3** was noted. The reduction onset potentials ($E_{red}^{onsetCV}$) were registered in the range of −1.76 to −2.18 V, with the lowest potential for **Az-4** and the highest potential for **Az-3**. Using the DPV method, the reduction of the imine bond was measured from −2.47 V (**Az-1**) to −2.29 V (**Az-4**).[13,41] For **Az-3** and **Az-5**, the lack of −CH═N− bond reduction was observed (cf. Figure S4), which may be related to the electrochemical window of the used solvent (i.e., CH_2Cl_2).

The first reduction process as well as the first oxidation process can be assigned to radical formation related to the thiophene ring reduction.[13]However, the first reduction process for **Az-5** can be assigned to the quinoline part.[42−46] Furthermore, in the case of oxidation of **Az-2**−**Az-4** based on DOS composition, the substituents play an important role and a similar value of the E_{ox}^{onset} may be associated with presence of nitrogen in the substituent chemical structure. Thiophene imine materials with the electron donor $-NH_2$ have shown low oxidation potentials compared to other structurally similar compounds.[10,13] The oxidation process is more difficult for compounds with one methyl group in the substituent (**Az-1**). For compounds with the electron accepting group of quinoline (**Az-5**), the reduction process occurs at a lower potential than for compounds with the electron donor $-CH_3$ group (cf. Table 1). An increase in the number of methyl groups and the presence of $-CH_2-CH_2$ groups shifted the E_{red} value to a higher potential (**Az-3** > **Az-2** > **Az-1**) (cf. Figure S4).

The electron affinities were obtained in the range from −2.92 to −3.28 eV and the ionization potentials in the range from −5.15 to −5.49 eV (cf. Table 2). Based on the CV method, the E_g value was between 1.81 and 2.44 eV.

3.4. Frontier Molecular Orbital Structure. Theoretical calculations were carried out with the use of DFT and the Gaussian09 program on the B3PW91/6-311g++ level. The molecular geometry of the singlet ground state of the imines was optimized in the gas phase with the Integral Equation Formalism variant of Polarizable Continuum Model (IEFPCM) and in dichloromethane for comparison of the HOMO and LUMO energies with electrochemical data. Such calculations were performed for the analysis of the frontier molecular orbital structure and energy levels. The optimized geometries of the imines are depicted in the Supporting Information Figures S5 and S6 presents the experimental and calculated IR spectra. Vibrational frequency calculations were carried out for each of these imines, to ensure that the optimized geometries represented the local minima of the

Table 2. Redox Properties (E_{ox}, E_{red} vs Fc/Fc^+), Ionization Potentials (IPs), Electron Affinities (EAs), and Energy Band Gap (E_g) with the HOMO and LUMO Estimated Using DFT of the Investigated Imines[a]

code	Az-1		Az-2		Az-3		Az-4		Az-5	
method	CV	DPV	CV	DPV	CV	DPV	CV	DPV	CV	DPV
E_{ox}^{onset} [V]	0.39	0.35	0.09	0.06	0.09	0.04	0.05	0.03	0.26	0.20
E_{ox} [V]	0.50	0.45	0.20	0.17	0.20	0.17	0.21	0.16	0.45	0.35
IP [eV]	−5.49	−5.45	−5.19	−5.16	−5.19	−5.14	−5.15	−5.13	−5.36	−5.30
E_{red}^{onset} [V]	−2.05	−2.04	−2.10	−2.15	−2.18	−2.20	−1.76	−1.80	−1.82	−1.90
E_{red} [V]	−2.18	−2.13	−2.24	−2.28	−2.32	−2.31	−1.90	−1.88	−1.95	−1.99
EA [eV]	−3.05	−3.06	−3.00	−2.95	−2.92	−2.90	−3.34	−3.30	−3.28	−3.20
E_g [eV]	2.44	2.39	2.19	2.21	2.27	2.24	1.81	1.83	2.08	2.10
$E_{red}^{-CH=N-}$ [V]	nd	−2.47	nd	−2.57	nd	nd	nd	−2.29	nd	nd
$HOMO^{DFT}$ [eV]	−5.60		−5.23		−5.33		−5.35		−5.69	
$LUMO^{DFT}$ [eV]	−2.13		−1.84		−1.93		−1.94		−2.47	
E_g^{DFT} [eV]	3.48		3.39		3.40		3.39		3.22	

[a]IP (eV) = $(-5.1 - E_{ox}^{onset})$·lel. EA (eV) = $(-5.1 - E_{red}^{onset})$·lel. $E_g = E_{ox}^{onset} - E_{red}^{onset}$. E_g^{DFT} = HOMO − LUMO. nd − not detected. Pt as the working electrode, v = 0.1 V/s, electrolyte 0.1 mol/dm^3 Bu_4NPF_6 in CH_2Cl_2, c = 10^{-4} mol/dm^3.

https://dx.doi.org/10.1021/acs.energyfuels.0c01698
Energy Fuels XXXX, XXX, XXX−XXX

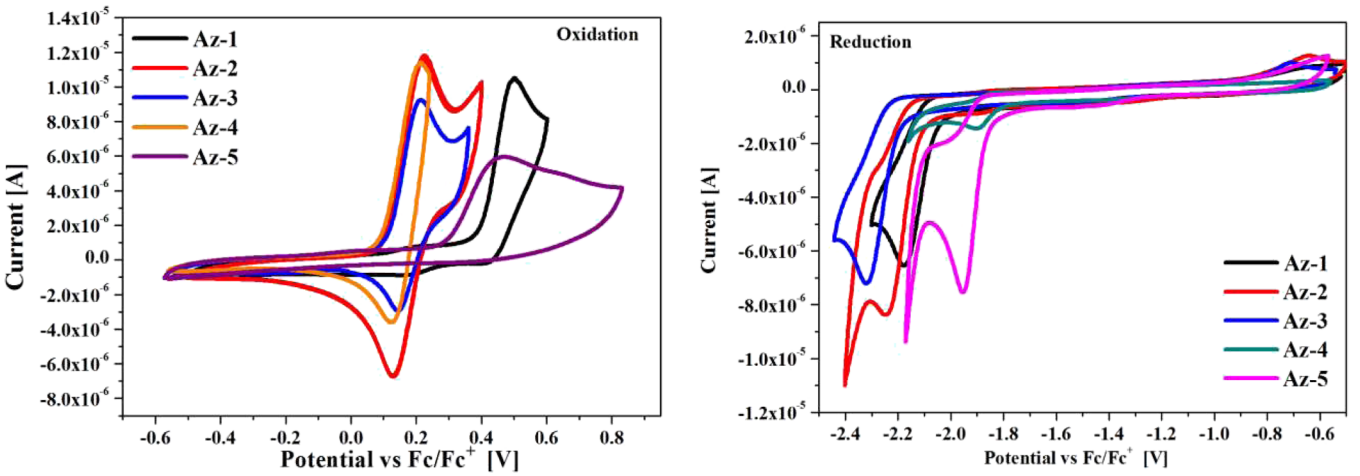

Figure 3. CV voltammograms of thiophene imine materials (Pt, v = 0.1 V/s, 0.1 mol/dm^3 Bu_4NPF_6 in CH_2Cl_2, c = 10^{-4} mol/dm^3).

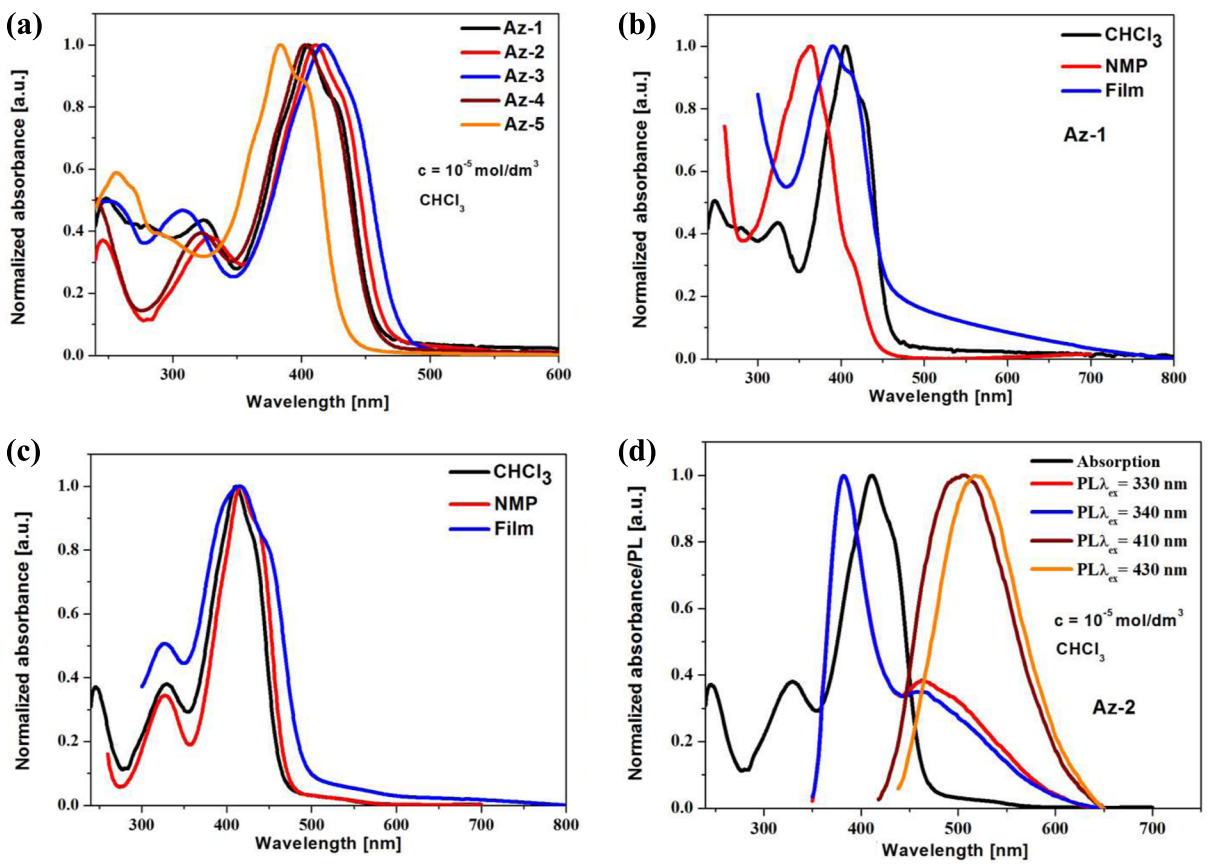

Figure 4. UV−vis spectra of **Az-1**−**Az-5** in (a) $CHCl_3$, (b) **Az-1**, and (c) **Az-2** in $CHCl_3$, NMP, and film, and (d) UV−vis spectra of **Az-1** in the $CHCl_3$ solution with different excitation wavelengths.

potential energy surface and that only positive eigenvalues were observed. In the ground state, the imines display the deviation from planarity and the mean plane angle between the thiophene and substituted phenyl is close to 35°, except for the **Az-5** molecule in which the angle is equal to 29.18° (cf. Table S4 in the Supporting Information).

Comparing the energies of HOMOs and LUMOs determined on the basis of the electrochemical data (cf. Table 2) with the theoretically calculated values, it can be observed that the calculated HOMO energies correspond well with the experimental values of IP determined from CV measurements. The miscalculations in the LUMO energy values are larger, with the calculated LUMO values being higher in energy than those determined experimentally. On the other hand, the calculated values of the HOMO and LUMO energies were used only for consistency with geometry optimization. For a more detailed description of the molecular orbitals, the contribution of molecule parts, i.e., substituted thiophene fragment, −CH═N−, and substituted phenyl moiety, to a molecular orbital was calculated using the GaussSum 3.0 program. The DOS diagrams are presented in Figure S7 in the Supporting Information and the composition

https://dx.doi.org/10.1021/acs.energyfuels.0c01698
Energy Fuels XXXX, XXX, XXX−XXX

of selected molecular orbitals is provided in Table S1 in the Supporting Information. The calculations show that the electronic density of the LUMO comprises the whole molecule, although the −HC═N− part plays a significant role in the energy level. The HOMO is mainly localized on the thiophene structure.

3.5. Optoelectronic and Emission Properties. The optoelectronic and emission properties of the synthesized imines were investigated via UV−vis and PL investigations supported by TD-DFT calculations (Gaussian 09 program on the B3PW91/6-311g++ level). The electronic absorption and PL spectra results were obtained in solvents such as *N*-methyl-2-pyrrolidone (NMP) and chloroform ($CHCl_3$) with different polarities. The optical properties in thin films on glass substrates were also studied. Electronic structures and electronic transitions were calculated with the IEFPCM using chloroform and NMP as solvents. The absorption data are provided in Table S2 in the Supporting Information. The UV−vis representative spectra are presented in Figure 4.

In the UV−vis spectra of the imines, the absorption band, with the maximum wavelength (λ_{max}) located in the range of 383−426 nm, considered as the $S_0 \rightarrow S_1$ transition, clearly dominates.[13] The λ_{max} in higher energy (241−295 nm) can be attributed to the $\pi-\pi^*$ transitions in the aromatic ring. The calculated UV−vis spectra correspond very well with the experimental one (cf. Figure S8). According to the TD-DFT calculations, the S_1 state corresponds to the HOMO→LUMO, whereas the S_2 state corresponds to the H-1/HOMO→LUMO/L+1/+2 transition (cf. Table S3 in the Supporting Information). Based on the data collected in Table S1 and DOS diagrams shown in Figure S7, the $S_0 \rightarrow S_1$ has a $\pi_{Th} \rightarrow \pi^*$ character, whereas $S_0 \rightarrow S_2$ in the case of **Az-2**, **Az-3**, and **Az-4** is associated with the $\pi_R \rightarrow \pi^*$transition and in the case of **Az-1** and **Az-5** has the same character as the lowest energy absorption band. Based on calculations, it was found that all molecules are polar. **Az-1** exhibits lower polarity than others and the dipole moment change in strongly polar NMP solution compared to chloroform is small.**Az-1** in NMP exhibited the hypsochromic shift of λ_{max} relative to $CHCl_3$ solution (cf. Figure 4b). In the case of **Az-2**, **Az-4**, and **Az-5**, the small solvatochromic effect, that is, the bathochromic shift of λ_{max} together with the solvent polarity increase was seen (cf. Figure S9). The molecules in thin films were more planar than those in solution, which led to increased conjugation, and the absorption bands were bathochromically shifted, although the shift was relatively small (cf. Figures S10 and S11).

Considering the PL studies, it was found that the investigated imines showed weak ability for light emission in solution with the quantum PL yield (Φ_{PL}) below 1%. Imines with the dimethylamino substituent in chloroform (**Az-2**) showed the highest Φ_{PL} (0.92%).As thin films on glass substrates, azomethines were nonemissive, except for **Az-2** (cf. Table S2). Generally, thiophene materials were practically weak or nonemissive in the solid state.[13]

It was found that the position of the maximum PL band (λ_{em}) was dependent on the excitation wavelengths (λ_{ex}) in violation of Kasha's rule due to the fluorescence emission from the second excited singlet state S_2. Both kinds of emission from S_2 and S_1 to S_0 were observed (cf. Figure 4d and Figure S12).[13]

At longer excitation wavelengths (corresponding to the $S_1 \rightarrow S_0$ transition), the PL intensity was very weak. The optimization of the first and second singlet excited state geometry was performed. Unfortunately, it was not possible to optimize the geometry of the S_1 state of these compounds in the gas phase as well as in $CHCl_3$ and NMP solutions. The optimization of the S_2 state for **Az-1**, **Az-2**, and **Az-3** also failed. The geometries of the second singlet excited states for **Az-4** and **Az-5** were optimized in $CHCl_3$ solution at the TD-B3PW91/6-311G++ level. The problem with the geometry optimization of the first excited state may indicate that the S_1 state is unstable and easily undergoes the nonradiative energy dissipation. Thus, the imines show weak emission from the first excited state. In the S_2 state, the molecular planarity distortion in the case of **Az-5** is much larger than in the ground state (cf. Table S4 in Supporting Information), which has a significant impact on the delocalization and conjugation of π-electrons in the molecules. The planarity of **Az-4** molecules is less disturbed in the S_2 state than in the ground state. Therefore, the quantum efficiency of **Az-4** is higher compared to that of **Az-5**. In the excited state, the polarity of **Az-4** and **Az-5** molecules is greater than in the S_0 state, which corresponds to the bathochromic shift of the emission maximum in NMP relative to chloroform solution (cf. Table S2).

3.6. Perovskite Solar Cells. In the present paper, to the best of our knowledge, for the first time thiophene imines obtained from DAT were investigated as HTMs in PCSs. The unencapsulated devices with the architecture FTO/b-TiO_2/m-TiO_2/perovskite/imine/Au were fabricated under ambient air with a humidity of 65% at 30−35 °C (cf. Figure 5). Additionally, the device without an HTM as a reference was constructed. The detailed process of PCS construction is given in the Experimental section.

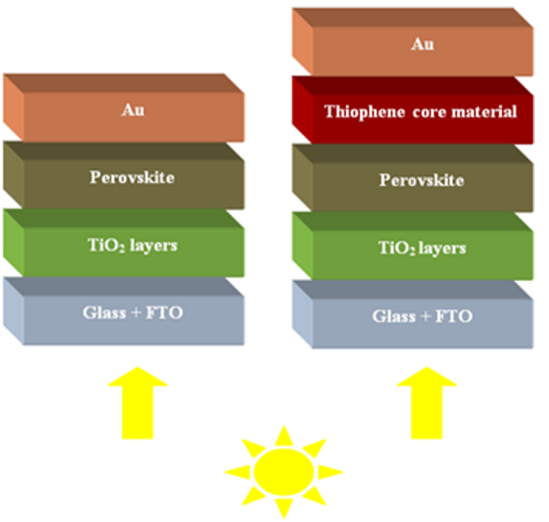

Figure 5. Scheme of the fabricated perovskite solar cells.

The calculated IP of imines being close to the HOMO level (cf. Table 2) was more positive than that of the valance band of $MAPbI_3$ (−5.43 eV). On the other hand, the EA of imines close to their LUMO level was relatively higher than the conductive band of the perovskite (−3.93 eV).[35] These findings suggest that the hole of the perovskite can transfer into the HOMO of azomethines and the electron reflux from perovskite to the counter electrode under illumination can be blocked. Thus, the imines have the potential to act as HTMs in PCS devices. The current−voltage ($I-V$) characteristics of the prepared solar cells were measured (Figure S14), and the photovoltaic parameters, J_{sc} − short-circuit current, V_{oc} −

https://dx.doi.org/10.1021/acs.energyfuels.0c01698
Energy Fuels XXXX, XXX, XXX−XXX

Table 3. Short-Circuit Current, Open-Circuit Voltage, and Other Photovoltaic Properties of the Prepared Perovskite Solar Cells

device structure	I_{sc} [mA]	J_{sc} [mA/cm^2]	V_{oc} [mV]	FF [−]	PCE [%]
FTO/b-TiO_2/m-TiO_2/perovskite/Au					
champion	0.36	1.45	430.6	0.25	0.17
forward	0.35 ± 0.06	1.42 ± 0.23	420.7 ± 66.4	0.25 ± 0.01	0.16 ± 0.05
backward	0.40 ± 0.03	1.58 ± 0.10	483.4 ± 40.6	0.26 ± 0.01	0.21 ± 0.03
FTO/b-TiO_2/m-TiO_2/perovskite/Az-1/Au					
champion	2.22	8.89	459.8	0.29	1.25
forward	2.31 ± 0.03	9.24 ± 0.14	462.4 ± 15.3	0.28 ± 0.01	1.24 ± 0.03
backward	1.74 ± 0.02	6.95 ± 0.09	354.6 ± 0.4	0.30 ± 0.01	0.77 ± 0.01
FTO/b-TiO_2/m-TiO_2/perovskite/Az-2/Au					
champion	1.09	4.37	547.9	0.29	0.74
forward	1.29 ± 0.40	5.15 ± 1.60	525.1 ± 49.3	0.25 ± 0.07	0.72 ± 0.06
backward	0.82 ± 0.02	3.28 ± 0.06	506.0 ± 46.2	0.33 ± 0.02	0.59 ± 0.07
FTO/b-TiO_2/m-TiO_2/perovskite/Az-3/Au					
champion	0.91	3.63	444.1	0.30	0.50
forward	0.93 ± 0.03	3.73 ± 0.13	450.6 ± 18.0	0.29 ± 0.04	0.50 ± 0.02
backward	0.65 ± 0.01	2.60 ± 0.05	338.4 ± 0.9	0.26 ± 0.01	0.24 ± 0.01
FTO/b-TiO_2/m-TiO_2/perovskite/Az-4/Au					
champion	2.05	8.20	579.3	0.32	1.59
forward	2.02 ± 0.07	8.10 ± 0.27	569.6 ± 19.5	0.32 ± 0.01	1.51 ± 0.16
backward	1.42 ± 0.02	5.70 ± 0.09	471.2 ± 9.6	0.36 ± 0.01	1.02 ± 0.04
FTO/b-TiO_2/m-TiO_2/perovskite/Az-5/Au					
champion	0.72	2.89	750.9	0.39	0.89
forward	0.70 ± 0.04	2.81 ± 0.17	750.4 ± 1.1	0.39 ± 0.01	0.85 ± 0.08
backward	0.51 ± 0.04	2.02 ± 0.17	729.7 ± 0.8	0.38 ± 0.02	0.58 ± 0.07

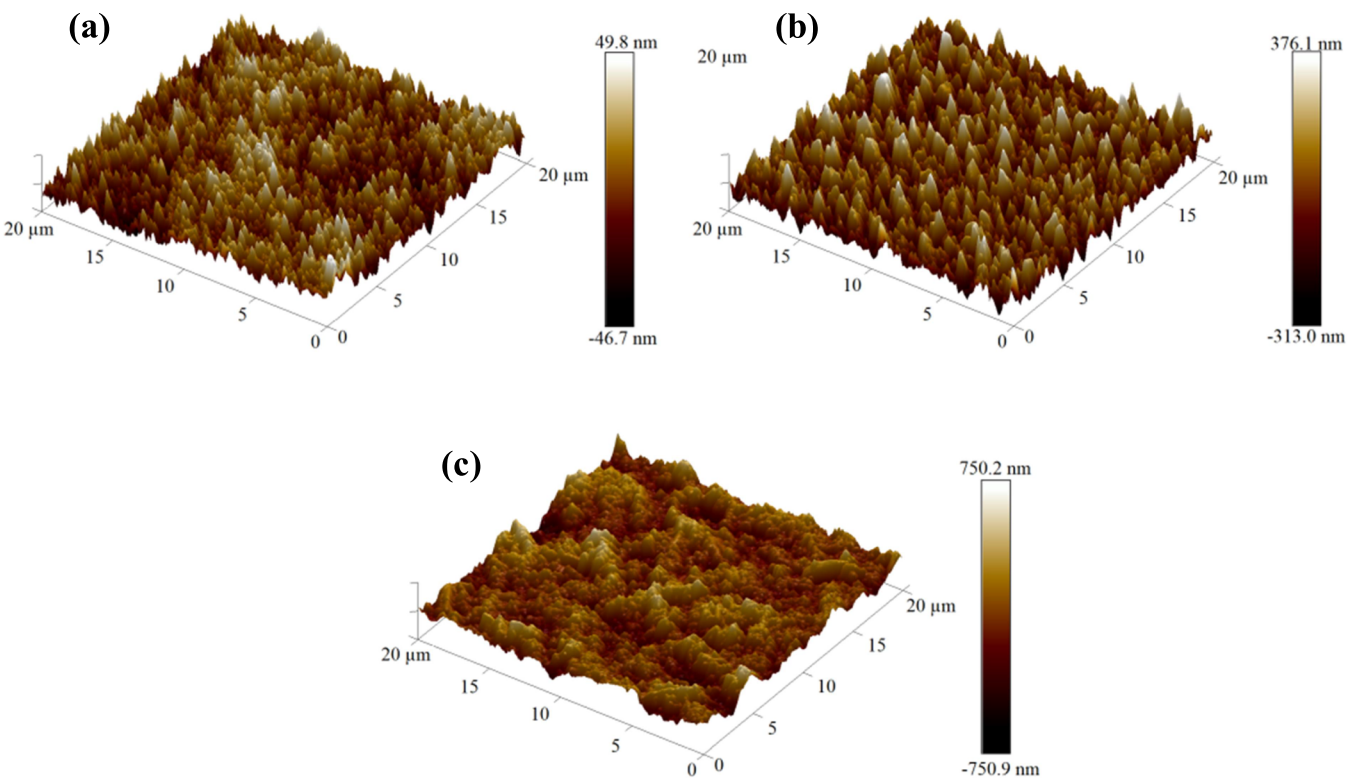

Figure 6. AFM micrographs of (a) TiO_2 onto FTO, (b) FTO/b-TiO_2/m-TiO_2/perovskite/, and (c) FTO/b-TiO_2/m-TiO_2/perovskite/**Az-4**.

open-circuit voltage, FF − fill factor, and PCE − power conversion efficiency, were calculated (cf. Table 3).

Considering the $J-V$ characteristics registered in a forward and reverse scan, it was found that the curves suffered from a severely large hysteresis (cf. Figure S14), which often appears in the case of PSCs and significantly has an impact on PV parameters. The origin of hysteresis is an aspect of debate and different assumptions are taken into account. Hysteresis is mainly related to the perovskite material, electron and hole transport layers, and the device architectures as well as it is

https://dx.doi.org/10.1021/acs.energyfuels.0c01698
Energy Fuels XXXX, XXX, XXX−XXX

dependent on the external scanning parameters.[47−49] The reduction or elimination of the hysteresis effect is necessary to achieve stable and reliable PSCs, and special attempts, which can reduce the hysteresis index have been made.[50,51] In case of fabricated devices the PCE was lower in the range of 0.15−0.57% than that of forward scan, which is not high differences, however considering the reached low value is significant.

It was found that devices bearing the imines showed better PV parameters compared to the reference cell FTO/b-TiO_2/m-TiO_2/perovskite/Au. A better efficiency resulted from the J_{SC} value, which mainly depends on the absorption of light. Thus, it was found that the devices with tested imines significantly differ in the incident photon-to-current efficiency (IPCE); unfortunately such measurements were not carried out. Moreover, it was found that the thicknesses of both the perovskite and HTM layers are also crucial for the calculation of J_{sc}, and thickness optimization for each layer is required.[52] If the thickness is less than the ideal thickness, the HTL may not cover the protruding perovskite crystals completely, which is present in the perovskite layer. The film-forming ability of the presented compounds may be different, which has an impact on its quality and thickness and finally on the J_{sc}. The film-forming capability of **Az-4** on the perovskite was investigated by atomic force microscopy (AFM). Additionally, the TiO_2 layers with and without perovskite were examined by AFM (cf. Figure 6).

The AFM results illustrate the root-mean-square (RMS) roughness values of the investigated layers. The micrographs indicate that the TiO_2 layers deposited onto FTO were very planar with an RMS value of about 15 nm in contrast to TiO_2 covered with the perovskite, which showed an RMS value of around 100 nm. The **Az-4** film spin-coated on the top of perovskite causes a significant decrease in the surface roughness to 50 nm. Thus, **Az-4** can create a very smooth capping layer on the perovskite and could form a better interfacial contact of perovskite/HTM/Au. The RMS value of the perovskite covered with **Az-4** is still relatively rough. Considering the absorption ability of **Az-4** in the visible range, it would create minor competitive absorption with the perovskite layer for light harvesting in devices (cf. Figure S15).

4. CONCLUSIONS

In conclusion, this work focuses on the investigations of five new thiophene imines toward optoelectronics. The relationships between the chemical structures of the synthesized azomethines and their selected properties crucial for applications were studied. It was found that:

- azomethines with the (cyanoethyl)methylamine, morpholine, and quinoline structure were thermally stable at 260 °C compared to imines with methyl and dimethylamine units;
- the substitution of the phenyl group with the methyl group (**Az-1**) and the introduction of the quinoline unit (**Az-5**) lowered the ionization potential compared to other substituents, and other imines showed the same IP value;
- the imines with an electron-donating unit exhibited the maximum absorption in the range of 401−433 nm and the substitution of the phenyl ring with amine derivatives (dimethylamine (**Az-2**) and (cyanoethyl)-methylamine (**Az-3**)) shifted λ_{max} to a lower energy. The introduction of the electron-acceptor group (quinoline) (**Az-5**) hypsochromically shifted λ_{max} to 383 nm;
- imines showed weak ability for photoluminescence with the quantum PL yield below 1% and both kinds of emission from S_2 and S_1 to S_0 were seen. Only **Az-2** was emissive in the solid state as the film,
- all imines showed the same activities as HTMs in PSCs and the compounds with the morpholine derivative (**Az-4**) showed the highest power conversion efficiency.

The presented imines can be considered as materials for further modification due to the presence of free amine groups, and **Az-4** is the most promising for such activities.

■ ASSOCIATED CONTENT

Supporting Information

The Supporting Information is available free of charge at https://pubs.acs.org/doi/10.1021/acs.energyfuels.0c01698.

Materials; structural characterizations; theoretical calculations; ^{1}H NMR and ^{13}C NMR of thiophene core materials; Potential energy profiles along the rotation of the $-NH_2$ group in the **Az-3** and **Az-5** azomethines; TGA curves; DPV voltammograms of thiophene core materials; molecular geometries of Az-x compounds in the ground state; normalized experimental and calculated IR spectra; composition of the selected molecular orbitals in the ground state; DOS diagrams; electronic absorption and photoluminescence data of the thiophene azomethines; experimental and calculated UV-vis spectra in $CHCl_3$ solution; calculated electronic transitions; absorption spectra of the **Az-1**−**Az-5** in $CHCl_3$ and NMP solutions and in the solid state in films; PL spectra of the **Az-1**−**Az-5**; geometrical parameters of Az-x molecules in the ground state; current−voltage (I−V) characteristics of the tested devices; and UV−vis absorption spectra of FTO/b-TiO_2/m-TiO_2/perovskite/**Az-4**/Au (PDF)

■ AUTHOR INFORMATION

Corresponding Author

Ewa Schab-Balcerzak − *Institute of Chemistry, University of Silesia, 40-006 Katowice, Poland; Centre of Polymer and Carbon Materials, Polish Academy of Sciences, 41-819 Zabrze, Poland;* orcid.org/0000-0002-7219-8664; Email: ebalcerzak@cmpw-pan.edu.pl, ewa.schab-balcerzak@us.edu.pl

Authors

Agnieszka Katarzyna Pająk − *Institute of Chemistry, University of Silesia, 40-006 Katowice, Poland*

Paweł Gnida − *Centre of Polymer and Carbon Materials, Polish Academy of Sciences, 41-819 Zabrze, Poland;* orcid.org/0000-0003-3350-9383

Sonia Kotowicz − *Institute of Chemistry, University of Silesia, 40-006 Katowice, Poland*

Jan Grzegorz Malecki − *Institute of Chemistry, University of Silesia, 40-006 Katowice, Poland*

Marcin Libera − *Institute of Chemistry, University of Silesia, 40-006 Katowice, Poland*

Katarzyna Bednarczyk − *Institute of Chemistry, University of Silesia, 40-006 Katowice, Poland*

Complete contact information is available at: https://pubs.acs.org/10.1021/acs.energyfuels.0c01698

https://dx.doi.org/10.1021/acs.energyfuels.0c01698
Energy Fuels XXXX, XXX, XXX−XXX

Notes

The authors declare no competing financial interest.

■ ACKNOWLEDGMENTS

This work was supported by the National Science Centre of Poland Grant: No. 2018/31/B/ST8/03294. The GAUSSIAN-09 calculations were carried out in the Wrocław Centre for Networking and Supercomputing, WCSS, Wrocław, Poland, http://www.wcss.wroc.pl (grant No. 18).

■ REFERENCES

(1) Azrain, M. M.; Mansor, M. R.; Fadzullah, S. H. S. M.; Omar, G.; Sivakumar, D.; Lim, L. M.; Nordin, M. N. A. Analysis of mechanisms responsible for the formation of dark spots in organic light emitting diodes (OLEDs): A review. *Synth. Met.* **2018**, *235*, 160−175.

(2) De Jong, F.; Daniels, M.; Vega-Castillo, L.; Kennes, K.; Martín, C.; De Miguel, G.; Cano, M.; Pérez-Morales, M.; Hofkens, J.; Dehaen, W.; Van der Auweraer, M. 10-Dihydrobenzo[a]indolo[2, 3-c]-carbazoles as Novel OLED Emitters. *J. Phys. Chem. B* **2019**, *123*, 1400−1411.

(3) Pluczyk, S.; Kuznik, W.; Lapkowski, M.; Reghu, R. R.; Grazulevicius, J. V. The effect of the linking topology on the electrochemical and spectroelectrochemical properties of carbazolyl substituted perylenebisimides. *Electrochim. Acta* **2014**, *135*, 487−494.

(4) Ohtani, S.; Gon, M.; Tanaka, K.; Chujo, Y. Construction of the Luminescent Donor−Acceptor Conjugated Systems Based on Boron-Fused Azomethine Acceptor. *Macromolecules* **2019**, *52*, 3387−3393.

(5) Burlov, A. S.; Vlasenko, V. G.; Koshchienko, Y. V.; Makarova, N. I.; Zubenko, A. A.; Drobin, Y. D.; Fetisov, L. N.; Kolodina, A. A.; Zubavichus, Y. V.; Trigub, A. L.; Levchenkov, S. I.; Garnovskii, D. A. Synthesis, characterization, luminescent properties and biological activities of zinc complexes with bidentate azomethine Schiff-base ligands. *Polyhedron* **2018**, *154*, 65−76.

(6) Temizkan, K.; Kaya, İ. Synthesis of soluble poly(azomethine)s containing thiophene and their fluorescence quantum yields. *Polym. Bull.* **2020**, *77*, 3287−3303.

(7) Yang, C. J.; Jenekhe, S. A. Conjugated aromatic poly-(azomethines). 1. Characterization of structure, electronic spectra, and processing of thin films from soluble complexes. *Chem. Mater.* **1991**, *3*, 878−887.

(8) Barik, S.; Bletzacker, T.; Skene, W. G. π-Conjugated fluorescent azomethine copolymers: opto-electronic, halochromic, and doping properties. *Macromolecules* **2012**, *45*, 1165−1173.

(9) Bolduc, A.; Mallet, C.; Skene, W. G. Survey of recent advances of in the field of π-conjugated heterocyclic azomethines as materials with tuneable properties. *Sci. China Chem.* **2013**, *56*, 3−23.

(10) Kotowicz, S.; Siwy, M.; Golba, S.; Malecki, J. G.; Janeczek, H.; Smolarek, K.; Szalkowski, M.; Sek, D.; Libera, M.; Mackowski, S.; Schab-Balcerzak, E. Spectroscopic, electrochemical, thermal properties and electroluminescence ability of new symmetric azomethines with thiophene core. *J. Lumin.* **2017**, *192*, 452−462.

(11) Kakekochi, V.; Kumar, U.; Chandrasekharan, K. An investigation on photophysical and third−order nonlinear optical properties of novel thermally−stable thiophene−imidazo [2, 1-b][1, 3, 4] thiadiazole based azomethines. *Dyes Pigm.* **2019**, *167*, 216−224.

(12) Bishop, S.; Tremblay, M. H.; Gellé, A.; Skene, W. G. Understanding Color Tuning and Reversible Oxidation of Conjugated Azomethines. *J. Phys. Chem. A* **2019**, *123*, 2687−2693.

(13) Gnida, P.; Pająk, A.; Kotowicz, S.; Malecki, J. G.; Siwy, M.; Janeczek, H.; Maćkowski, S.; Schab-Balcerzak, E. Symmetrical and unsymmetrical azomethines with thiophene core: structure−properties investigations. *J. Mater. Sci.* **2019**, *54*, 13491−13508.

(14) Tokárová, Z.; Maxianová, P.; Váry, T.; Nádaždy, V.; Végh, D.; Tokár, K. Thiophene-centered azomethines: Structure, photophysical and electronic properties. *J. Mol. Struct.* **2020**, *1204*, 127492.

(15) Shahab, S.; Sheikhi, M.; Filippovich, L.; Ihnatovich, Z.; Koroleva, E.; Drachilovskaya, M.; Atroshko, M.; Pazniak, A. Spectroscopic (FT-IR, excited states, UV/Vis, polarization) properties, synthesis and quantum chemical studies of new azomethine derivatives. *Dyes Pigm.* **2019**, *170*, 107647.

(16) Bogdanowicz, K. A.; Jewloszewicz, B.; Dysz, K.; Przybyl, W.; Dylong, A.; Mech, W.; Korona, K. P.; Skompska, M.; Kaim, A.; Kamińska, M.; Iwan, A. Electrochemical and optical studies of new symmetrical and unsymmetrical imines with thiazole and thiophene moieties. *Electrochim. Acta* **2020**, *332*, 135476.

(17) Petrus, M. L.; Bouwer, R. K. M.; Lafont, U.; Athanasopoulos, S.; Greenham, N. C.; Dingemans, T. J. Small-molecule azomethines: organic photovoltaics via Schiff base condensation chemistry. *J. Mater. Chem.* **2014**, *2*, 9474−9477.

(18) Demeter, D.; Mohamed, S.; Diac, A.; Grosu, I.; Roncali, J. Small molecular donors for organic solar cells obtained by simple and clean synthesis. *ChemSusChem* **2014**, *7*, 1046−1050.

(19) Sęk, D.; Siwy, M.; Małecki, J. G.; Kotowicz, S.; Golba, S.; Nowak, E. M.; Sanetra, J.; Schab-Balcerzak, E. Polycyclic aromatic hydrocarbons connected with Schiff base linkers: Experimental and theoretical photophysical characterization and electrochemical properties. *Spectrochim. Acta A* **2017**, *175*, 168−176.

(20) Sek, D.; Siwy, M.; Grucela, M.; Małecki, G.; Nowak, E. M.; Lewinska, G.; Santera, J.; Laba, K.; Lapkowski, M.; Kotowicz, S.; Schab-Balcerzak, E. New anthracene-based Schiff bases: Theoretical and experimental investigations of photophysical and electrochemical properties. *Spectrochim. Acta A* **2017**, *175*, 24−35.

(21) Iwan, A.; Boharewicz, B.; Tazbir, I.; Sikora, A.; Schab-Balcerzak, E.; Grucela-Zajac, M.; Skorka, Ł. Structural and electrical properties of mixture based on P3HT: PCBM and low band gap naphthalene diimide-imines. *Synth. Met.* **2014**, *189*, 183−192.

(22) Nowak, E. M.; Sanetra, J.; Grucela, M.; Schab-Balcerzak, E. Azomethine naphthalene diimides as component of active layers in bulk heterojunction solar cells. *Mater. Lett.* **2015**, *157*, 93−98.

(23) Iwan, A.; Schab-Balcerzak, E.; Korona, K. P.; Grankowska, S.; Kamińska, M. Investigation of optical and electrical properties of new aromatic polyazomethine with thiophene and cardo moieties toward application in organic solar cells. *Synth. Met.* **2013**, *185-186*, 17−24.

(24) Petrus, M. L.; Bouwer, R. K. M.; Lafont, U.; Murthy, D. H. K.; Kist, R. J. P.; Böhm, M. L.; Olivier, Y.; Savenije, T. J.; Siebbeles, L. D. A.; Greenham, N. C.; Dingemans, T. J. Conjugated poly(azomethine) s via simple one-step polycondensation chemistry: synthesis, thermal and optoelectronic properties. *Polym. Chem.* **2013**, *4*, 4182−4191.

(25) Kwon, J.; Lee, W.; Kim, J. Y.; Noh, S.; Lee, C.; Hong, J. I. Solution processable donor materials based on thiophene and triphenylamine for bulk heterojunction solar cells. *New J. Chem.* **2010**, *34*, 744−749.

(26) Pokhrel, B., Dolui, S. K., Synthesis, characterization and photovoltaic property evaluation of poly (3-phenyl azomethine alkyl thiophene)s. In *National Conference on Recent Advances in Civil Engineering (NCRACE-2013, 15−16 November), Int. J. Innovative Res. Sci. Eng. Technol*, 2014, 3: 184−189.

(27) Gao, Z.; Guo, L.; Sun, Y.; Qu, W.; Yang, T.; Li, B.; Li, J.; Duan, L. Passivating ZnO with a naphthalimide-Schiff base as electron transport layer for inverted polymer solar cells. *Org. Electron.* **2019**, *67*, 232−236.

(28) Iwan, A.; Boharewicz, B.; Parafiniuk, K.; Tazbir, I.; Gorecki, L.; Sikora, A.; Filapek, M.; Schab-Balcerzak, E. New air-stable aromatic polyazomethines with triphenylamine or phenylenevinylene moieties towards photovoltaic application. *Synth. Met.* **2014**, *195*, 341−349.

(29) Iwan, A.; Palewicz, M.; Krompiec, M.; Grucela-Zajac, M.; Schab-Balcerzak, E.; Sikora, A. Synthesis, materials characterization and opto(electrical) properties of unsymmetrical azomethines with benzothiazole core. *Spectrochim. Acta A* **2012**, *97*, 546−555.

(30) Sarswat, P. K.; Sathyapalan, A.; Zhu, Y.; Free, M. L. Design, synthesis, and characterization of TPA-thiophene-based amide or imine functionalized molecule for potential optoelectronic devices. *J. Theor. Appl. Phys.* **2013**, *7*, 4.

(31) Petrus, M. L.; Bein, T.; Dingemans, T. J.; Docampo, P. A low cost azomethine-based hole transporting material for perovskite photovoltaics. *J. Mater. Chem. A* **2015**, *3*, 12159−12162.

https://dx.doi.org/10.1021/acs.energyfuels.0c01698
Energy Fuels XXXX, XXX, XXX−XXX

(32) Petrus, M. L.; Music, A.; Closs, A. C.; Bijleveld, J. C.; Sirtl, M. T.; Hu, Y.; Dingemans, T. J.; Bein, T.; Docampo, P. Design rules for the preparation of low-cost hole transporting materials for perovskite solar cells with moisture barrier properties. *J. Mater. Chem. A* **2017**, *5*, 25200−25210.
(33) Petrus, M. L.; Sirtl, M. T.; Closs, A. C.; Bein, T.; Docampo, P. Hydrazone-based hole transporting material prepared via condensation chemistry as alternative for cross-coupling chemistry for perovskite solar cells. *Mol. Syst. Des. Eng.* **2018**, *3*, 734−740.
(34) Gawlinska, K.; Iwan, A.; Starowicz, Z.; Kulesza-Matlak, G.; Stan-Glowinska, K.; Janusz, M.; Lipinski, M.; Boharewicz, B.; Tazbir, I.; Sikora, A. Searching of new, cheap, air-and thermally stable hole transporting materials for perovskite solar cells. *Opto-Electron Rev* **2017**, *25*, 274−284.
(35) Gawlińska-Nęcek, K.; Starowicz, Z.; Tavgeniene, D.; Krucaite, G.; Grigalevicius, S.; Schab-Balcerzak, E.; Lipiński, M. A solution-processable small-organic molecules containing carbazole or phenoxazine structure as hole-transport materials for perovskite solar cells. *Opto-Electron Rev.* **2019**, *27*, 137−142.
(36) Kula, S.; Pająk, A.; Szlapa-Kula, A.; Mieszczanin, A.; Gnida, P.; Lipiński, M.; Schab-Balcerzak, E. 9,9′-bifluorenylidene derivatives as novel hole-transporting materials for potential photovoltaic applications. *Dyes Pigm.* **2020**, *174*, 108031.
(37) Im, J.-H.; Jang, I.-H.; Pellet, N.; Grätzel, M.; Park, N.-G. Growth of $CH_3NH_3PbI_3$ cuboids with controlled size for high-efficiency perovskite solar cells. *Nat. Nanotechnol.* **2014**, *9*, 927.
(38) Bourgeaux, M.; Vomscheid, S.; Skene, W. G. Optimized Synthesis and Simple Purification of 2,5-Diamino-thiophene-3,4-dicarboxylic Acid Diethyl Ester. *Synth. Commun.* **2007**, *37*, 3551−3558.
(39) Han, Y.; Tang, W.-Q.; Yan, C. G. Gewald-type reaction of double activated 2,3-diarylcyclopropanes with elemental sulfur for synthesis of polysubstituted 2-aminothiophenes. *Tetrahedron Lett.* **2014**, *55*, 1441−1443.
(40) Bujak, P.; Kulszewicz-Bajer, I.; Zagorska, M.; Maurel, V.; Wielgus, I.; Pron, A. Polymers for electronics and spintronics. *Chem. Soc. Rev.* **2013**, *42*, 8895−8999.
(41) Dufresne, S.; Skene, W. G. Unsymmetric pyrrole, thiophene, and furan-conjugated comonomers prepared using azomethine connections: Potenatial new monomers for alternating homocoupled products. *J. Org. Chem.* **2008**, *73*, 3859−3866.
(42) Kotowicz, S.; Siwy, M.; Filapek, M.; Malecki, J. G.; Smolarek, K.; Grzelak, J.; Mackowski, S.; Slodek, A.; Schab-Balcerzak, E. New donor-acceptor-donor molecules based on quinoline acceptor unit with Schiff base bridge: synthesis and characterization. *J. Lumin.* **2017**, *183*, 458−469.
(43) Okumara, L. L.; Stradiotto, N. R. Simultaneous determination of quinoline and pyridine compounds in gasoline and diesel by differential pulse voltammetry. *Electroanalysis* **2007**, *19*, 709−716.
(44) Slodek, A.; Matussek, M.; Filapek, M.; Szafraniec-Gorol, G.; Szlapa, A.; Grudzka-Flak, I.; Szczurek, M.; Malecki, J. G.; Maron, A.; Schab-Balcerzak, E.; Nowak, E. M.; Sanetra, J.; Olejnik, M.; Danikiewicz, W.; Krompiec, S. Small donor-acceptor molecules based on quinoline-fluorene system with promising photovoltaic properties. *Eur. J. Org.* **2016**, *2016*, 2500−2508.
(45) Slodek, A.; Zych, D.; Maroń, A.; Golba, S.; Schab-Balcerzak, E.; Janeczek, H.; Siwy, M.; Maćkowski, S. Fluorene vs carbazole substituent at quinoline core toword organic electronics. *Dyes Pigm.* **2019**, *166*, 98−106.
(46) Slodek, A.; Zych, D.; Maroń, A.; Malecki, J. G.; Golba, S.; Szafraniec-Gorol, G.; Pajak, M. Does the length matter? - Synthesis, photophysical, and theoretical study of novel quinolines based on carbazoles with different length of alkyl chain. *Dyes Pigm.* **2019**, *160*, 604−613.
(47) Wu, F.; Pathak, R.; Chen, C.; Tong, Y.; Xu, H.; Zhang, T.; Jian, R.; Li, X.; Qiao, Q. Reduced hysteresis in perovskite solar cells using metal oxide/organic hybrid hole transport layer with generated interfacial dipoles. *Electrochim. Acta* **2020**, *354*, 136660.
(48) Yu, M.; Wang, H.-Y.; Zhao, J.-S.; Qin, Y.; Zhang, J.-P.; Ai, X.-C. The influence of fullerene on hysteresis mechanism in planar perovskite solar cells. *Chem. Phys. Lett.* **2020**, *750*, 137443.
(49) Hu, X.; Wang, H.; Wang, M.; Zang, Z. Interfacial defects passivation using fullerene-polymer mixing layer for planar-structure perovskite solar cells with negligible hysteresis. *Solar Ener.* **2020**, *206*, 816−825.
(50) Peng, L.; Liu, Z. Reduce the hysteresis effect with the PEIE interface dipole effect in the organic-inorganic hybrid perovskite $CH_3NH_3PbI_{3-x}Cl_x$ solar cell. *Org. Electr.* **2018**, *62*, 630−636.
(51) Jeon, N. J.; Noh, J. H.; Kim, Y. C.; Yang, W. S.; Ryu, S.; Seok, S. I. Solvent engineering for high-performance inorganic−organic hybrid perovskite solar cells. *Nat. Mater.* **2014**, *13*, 897−903.
(52) Bag, A.; Radhakrishnan, R.; Nekovei, R.; Jeyakumar, R. Effect of absorber layer, hole transport layer thicknesses, and its doping density on the performance of perovskite solar cells by device simulation. *Sol. Energy* **2020**, *196*, 177−182.

https://dx.doi.org/10.1021/acs.energyfuels.0c01698
Energy Fuels XXXX, XXX, XXX−XXX